Materials Advances

REVIEW

Check for updates

Molecularly imprinted photocatalysts: fabrication, application and challenges

Yaoyu Luo,†[a] Xinrui Feng,†[a] Zhiliang Chen[b] and Xiantao Shen ✦[a]

Targeted degradation of environmental pollutants (EPs) has attracted increasing attention in the field of environmental science. By integrating the advantages of both conventional photocatalysis and molecular imprinting, molecularly imprinted photocatalysts (MIPCs) are proposed for selective removal of target EPs. At present, how to design efficient MIPCs has become a timely research topic. Here, we review the comprehensive design and synthesis routes of MIPCs related to photocatalytic performance, including the selection of photocatalytic matrixes, templates, monomers, and cross-linkers. Also, various kinds of applications of selective photocatalysis by molecular imprinting are summarized, such as the fabrication of photoelectrochemical sensors and the photocatalytic degradation of target EPs based on the oxidation, reduction, and derivation systems. Finally, we discuss some potential challenges in the development of emerging MIPCs. The purpose of this review is to offer helpful guidance for the preparation of novel MIPCs and outlooks on the targeted monitoring and removal of environmental pollutants *via* MIPCs.

1. Introduction

Since the Honda–Fujishima effect was reported in 1972, plenty of photocatalytic materials with semiconducting properties have been synthesized and widely applied in environmental

[a] *State Key Laboratory of Environment Health (Incubation), Key Laboratory of Environment and Health, Ministry of Education, Key Laboratory of Environment and Health (Wuhan), Ministry of Environmental Protection, School of Public Health, Tongji Medical College, Huazhong University of Science and Technology, #13 Hangkong Road, Wuhan, Hubei, 430030, China.*
E-mail: xtshenlab@hust.edu.cn
[b] *Wuhan Prevention and Treatment Center for Occupational Diseases, Jianghan Bei Lu 18, Wuhan, Hubei, 430015, China*
† These authors contributed equally.

and energy fields.[1,2] Due to their suitable band-gap width and valence/conduction band position, TiO_2 semiconductors have been widely considered to prepare photocatalysts in the past few decades.[3] Moreover, for degradation of contaminants with advanced oxidation processes (AOPs) *via* photocatalysis, the anatase TiO_2-based photocatalyst is always more preferred than the other two polymorphs (the rutile and brookite) because of its photocatalytic activity.[4] Besides, to enhance photocatalytic performance, many original studies on the synthesis of photocatalysts using ZnO, CdSe, g-C_3N_4 or other nanomaterials as the photocatalytic matrix are reported.[5] However, because the degradation of environmental pollutants (EPs) by the AOPs is a hydroxyl radical reaction, the reaction selectivity of the AOPs is poor and of major global concern in the targeted degradation of EPs.[6–8]

Yaoyu Luo received the BS degree from Huazhong University of Science and Technology, China, in 2018. He is currently working toward the MS degree in Public Health with Tongji medical school of Huazhong University of Science and Technology. His research interests include molecular imprinting and selective photocatalysis, treatment of environmental pollutants, and sample pretreatment.

Yaoyu Luo

Xinrui Feng is a postgraduate working toward the MS degree in Public Health with Tongji medical school of Huazhong University of Science and Technology. She was awarded her BS degree in public health and preventive medicine by Southeast University, China, in 2019. Her research interests include treatment of environmental pollutants, environmental health, and population medicine.

Xinrui Feng
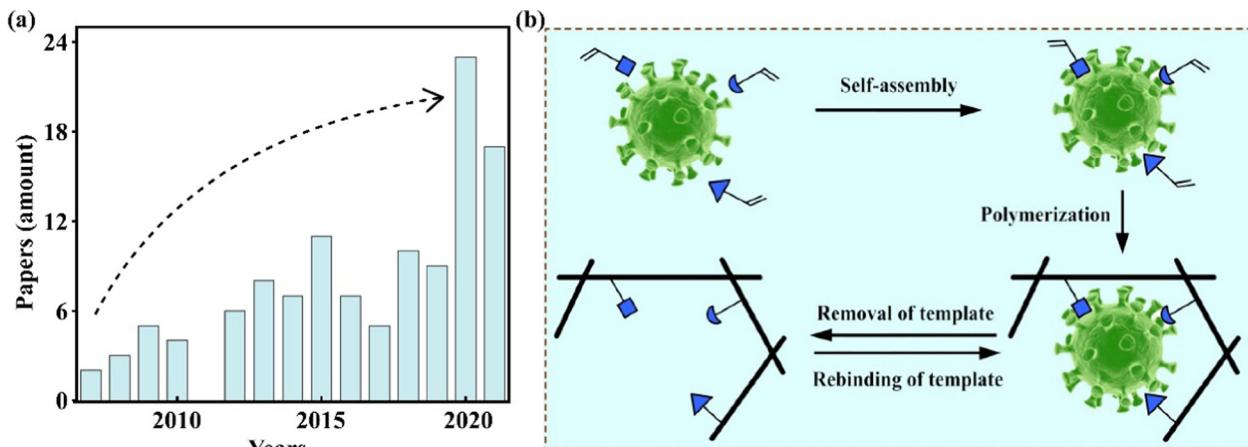
Fig. 1 (a) Amount of papers on photocatalysis based on molecular imprinting from the WOS data since 2007 to 2021. (b) Schematic representation of the synthesis of molecularly imprinted polymers (MIPs).

Molecular imprinting is a straightforward technique for the production of specific cavities on molecularly imprinted polymers (MIPs) using a template molecule.[9] Because of the high selectivity achieved by the template, MIPs have been widely used in chemical separation,[10,11] drug delivery,[12] plastic antibodies,[13] sensors,[14] and catalysis.[15] Recently, selective removal of EPs using molecular imprinting has gained considerable attention.[16] By combining the benefits of both AOPs and molecular imprinting, Shen et al. first developed an efficient approach for selective removal of EPs in 2007.[17] During photodegradation, a hybrid semiconductor photocatalyst grafted with a conductive MIP layer enhanced the photocatalytic decomposition of the EPs.[18]

With the past 15 years of development, hundreds of studies involving molecularly imprinted photocatalysts (MIPCs) have been reported.[19–23] As shown in Fig. 1(a), the number of publications reported in the web of science (WOS) has increased each year, especially in the last two years there has been a significant increase (over twice the amount). Therefore, a comprehensive overview of MIPCs from design to application will be significant to the researchers interested in this field. Accordingly, this review introduces the basic principles of molecular imprinting and selective photocatalysis. The design and synthesis routes of MIPCs related to photocatalytic performance are fully investigated, which included the selection of a suitable matrix, template, monomer, cross-linker etc. We also review various kinds of applications of selective photocatalysis by molecular imprinting, such as selective photocatalytic removal of organics, antibiotics, and metal ions based on conventional oxidation, reduction, and derivation systems, and especially highlight the fabrication of photoelectrochemical sensors for enhancing detection selectivity. Finally, some potential challenges to be overcome and efforts that should be made by researchers are discussed. We believe that this review offers helpful guidance for the preparation of novel MIPCs and outlooks on the targeted monitoring and removal of environmental pollutants via MIPCs.

Zhiliang Chen

Zhiliang Chen completed his PhD degree from Huazhong University of Science and Technology, China, in 2018. He carried out his postdoctoral research at Huazhong University of Science and Technology from 2018 to 2021 before moving to the Wuhan Prevention and Treatment Center for Occupational Diseases. His research interests include the preparation of molecularly imprinted polymers, metal pollutants degradation, and prevention of occupational diseases.

Xiantao Shen

Xiantao Shen is a full Professor at Huazhong University of Science and Technology. He received his PhD degree from Huazhong University of Science and Technology, China, in 2010. He worked in Lund University as a postdoctoral researcher from 2010 to 2012 and then moved to Mamlo University and worked as a guest researcher from 2013 to 2014. His research interests include the mechanism study of molecular imprinting, molecularly imprinted inorganic crystals, selective photocatalysis, and their applications in the field of environmental science and health.

2. Molecular imprinting and selective photocatalysis

The idea of molecular imprinting was put forward by Pauling during the study of the interaction between a protein antibody and an antigen in the 1940s.[24] Following this work, molecular imprinting has become a powerful technique for the synthesis of polymer matrices that function as synthetic receptors.[9] The schematic representation of the synthesis of MIPs is shown in Fig. 1(b). Typically, the functional monomers and the template initially form a complex by self-assembly. With an initiation, the complex in the presence of a cross-linker is polymerized. After removal of the template under certain conditions, cross-linked polymeric materials (named MIPs) are obtained.[13] It is known that the specific recognition ability of MIPs depends on the morphology and the functional groups of the template.[12] Hence, the template molecules should satisfy the following several requirements: they (i) should possess excellent chemical stability during the polymerization, (ii) should contain functional groups for imprinting, and (iii) should not contain groups involved in polymerization. In the literature, heavy metal ions, drugs, saccharides, peptides, proteins, cells, viruses, and bacteria have been successfully used as templates for molecular imprinting.[9,13]

Photocatalysis is a process of converting light energy into chemical energy by the photoexcitation of the valence electrons into the conduction band. The excited electrons (e^-) in the conduction band can reduce adsorbed chemicals on the surface of photocatalysts and the valence band holes (h^+) show oxidation, and the coupled e^- and h^+ are named charge carriers.[25,26] Thus, the photocatalytic performance is attributed to the separation of photogenerated electrons and holes. In other words, the width of the band gap and the position of the valence/conduction band are crucial factors for the photocatalytic properties. For example, a schematic representation of molecular orbital interactions between titanium (Ti) and oxygen (O) of anatase TiO_2 semiconductors is shown in Fig. 2(a), where the band gap is 3.20 eV.[27] For EP degradation using pure anatase TiO_2-based photocatalysts, different processes of the charge carriers can be carried out only under ultraviolet (UV) light ($\lambda \leq 387$ nm) irradiation (Fig. 2(b)). But the recombination of charge carriers generally wastes lots of energy ($>90\%$).

Moreover, during the redox reaction process of EP degradation, charge carriers can be transformed into different oxidants, such as hydroxyl radicals ($^\bullet OH$). As shown in the following eqn (1)–(9), with exposure to the $^\bullet OH$ radicals, EPs (like organics) could be completely mineralized into CO_2, H_2O, and mineral salts.

$$TiO_2 + h\nu \rightarrow e^- + h^+ \tag{1}$$

$$e^- + h^+ \rightarrow energy \tag{2}$$

$$h^+ + H_2O \rightarrow {}^\bullet OH + H^+ \tag{3}$$

$$h^+ + OH^- \rightarrow {}^\bullet OH \tag{4}$$

$$e^- + O_2 \rightarrow {}^\bullet O_2^- \tag{5}$$

$${}^\bullet O_2^- + H_2O \rightarrow {}^\bullet OOH + OH^- \tag{6}$$

$$2HO_2^\bullet \rightarrow H_2O_2 + O_2 \tag{7}$$

$$e^- + H_2O_2 \rightarrow {}^\bullet OH + OH^- \tag{8}$$

$${}^\bullet OH \ (or\ h^+) + organics \rightarrow CO_2 + H_2O \tag{9}$$
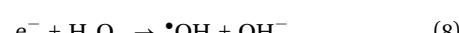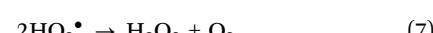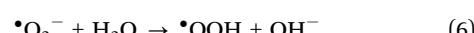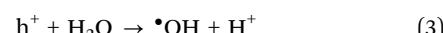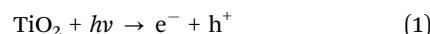
For EP degradation, superoxide radical anions ($^\bullet O_2^-$) reduced by e^- and molecular oxygen and hydroperoxyl radicals ($^\bullet OOH$) formed by the combination of $^\bullet O_2^-$ and H^+ play important roles, the same as that played by $^\bullet OH$, but only a small portion of charge carriers can be separated forming oxidants in a typical photocatalysis process.[28,29] Although ZnO, WO_3, ZnS, and CdS are also widely used to form photocatalysts, routine photocatalytic degradation in the liquid phase is non-selective because of the free radical mechanism.[30,31] These greatly limit the performance of photocatalysts for the removal of low-level EPs in the presence of high-level less harmful pollutants. Therefore, selective photocatalysis has received more attention in the past few decades. And many strategies to enhance the selectivity of TiO_2-based photocatalysts have been reported, including controlling the surface electric charge *via* adjusting the pH of reaction, coating the surface with specific molecules, adjusting the degree
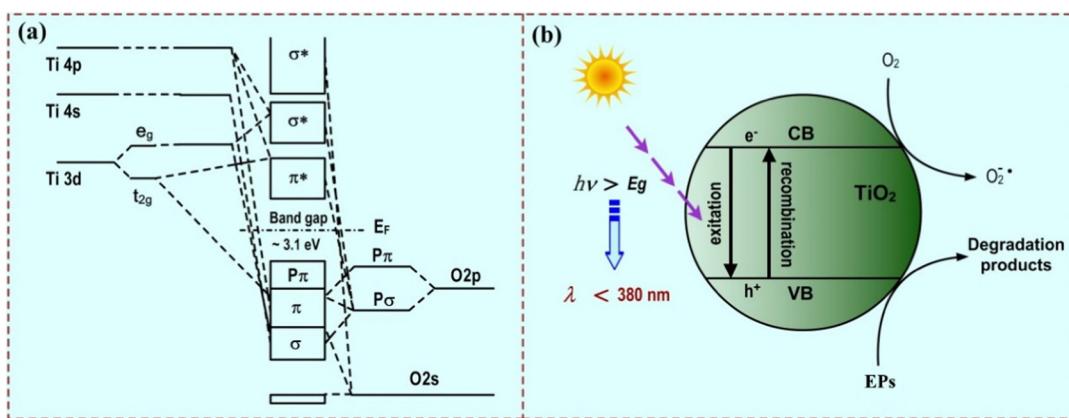

Fig. 2 (a) Schematic representation of molecular orbital interactions between titanium (Ti) and oxygen (O) of TiO_2 semiconductors. Adapted with permission from ref. 27. (b) Schematic representation of the photodegradation of EPs on TiO_2 semiconductors.

of {001} high-energy facets of crystals, and synthesizing double-region-structured photocatalysts.[32,33]

Besides, because of the high selectivity of molecular imprinting described above, a novel method to enhance the photocatalytic selectivity was developed by coating TiO_2 nanoparticles with a thin molecularly imprinted layer. The molecularly imprinted layer selectively concentrates the target molecules and the TiO_2 nanoparticles degrade the adsorbed target pollutants by the hydroxyl radicals.[17] Inspired by this work, several types of MIPCs have been developed and shown great potential for targeted monitoring and removal of EPs.

3. Fabrication of molecularly imprinted photocatalysts

3.1 Design fundamentals of molecularly imprinted photocatalysts

As mentioned above, a molecularly imprinted photocatalyst mainly consists of two key parts, namely a photocatalytic active center and a selective recognition region. Generally, the former is a matrix formed using various materials (such as semiconductors) with photocatalytic activity, and the latter is an imprinted cavity formed by MIPs. In order to achieve a combination of the two parts, by coating imprinted silica/alumina on the surface of TiO_2 nanoparticles, a molecularly imprinted photocatalyst with an MIP shell was prepared (Fig. 3(a)).[34]

Nowadays, many MIPCs are synthesized with sol–gel techniques.[35] A schematic route for the preparation of the MIPCs via an acid-catalyzed sol–gel process is shown in Fig. 3(b), in which TiO_2 (P25) is added after the mixture of tetraethoxysilane (TEOS) and HCl at a proper volume ratio reacts with model EPs. And to promote the biological application, some imprinted photocatalysts were synthesized using a biological hydrogel-based MIP matrix.[36–38] The structures of these hydrogels (calcium alginate, chitosan, and bacterial cellulose) used in imprinted photocatalysis are summarized in Fig. 4. Moreover, to enhance the photocatalytic performance, molecularly imprinted hollow TiO_2 microspheres were synthesized.[39] The imprinted hollow TiO_2 geometry was able to combine the sorption selectivity with the photonic efficiency typical of the hollow structure. In a word, due to the difference between the photocatalytic matrix and imprinting method, the photocatalytic performance of different MIPCs varies as well as the structure (including but not limited to a particle with a core–shell, a hollow microsphere, a nanotube with an imprinted layer/film, and an imprinted hydrogel). To better guide the design and synthesis of MIPCs, the factors related to performance are investigated below.

3.2 Using semiconductors as the photocatalytic matrix

During the synthesis of MIPCs, various types of semiconductors have been used as the photocatalytic matrix. Generally, according to the requirements for irradiating light, a suitable semiconductor must be taken into consideration. For example, MIPCs activated under UV light are usually synthesized by using single TiO_2[40,41] or ZnO[42,43] as the photocatalytic matrix. And for visible light irradiation, a semiconductor with a narrow forbidden band gap is a good choice, such as CdS, α-Fe_2O_3, Ag_3PO_4, or graphite carbon nitride (g-C_3N_4).[44–47] Recently, some ternary oxide semiconductors, represented by AFe_2O_4 types (A = Zn, Co, and Cu), have gotten much attention because of their excellent photochemical stability and rapid magnetic separation.[48–51]

Besides single semiconductors above, coupling a high-band gap semiconductor with a low-band gap semiconductor is an efficient way to increase the photocatalytic activity. For example, molecularly imprinted Dawson-type TiO_2/heteropolyacid cobalt(II) salt was prepared by the method of impregnation, stepwise acidification, and sol–gel.[52] The schematic mechanism of degradation of the target over the MIPCs is shown in Fig. 5. Compared to non-imprinted TiO_2, the imprinted TiO_2/heteropolyacid cobalt(II) salt showed an enhanced removal efficiency of the target by $\sim$33%. So far, by coupling other semiconductors (like Ag_2S,[19] WO_3,[53] Cu_2O,[54] reduced graphene oxide,[55] silylated graphene oxide,[56] graphene,[57] graphene oxide,[58] and carbon dots[59]), many TiO_2/ZnO-based nanocomposites have been successfully fabricated and employed as the photocatalytic matrix for the generation of novel MIPCs.
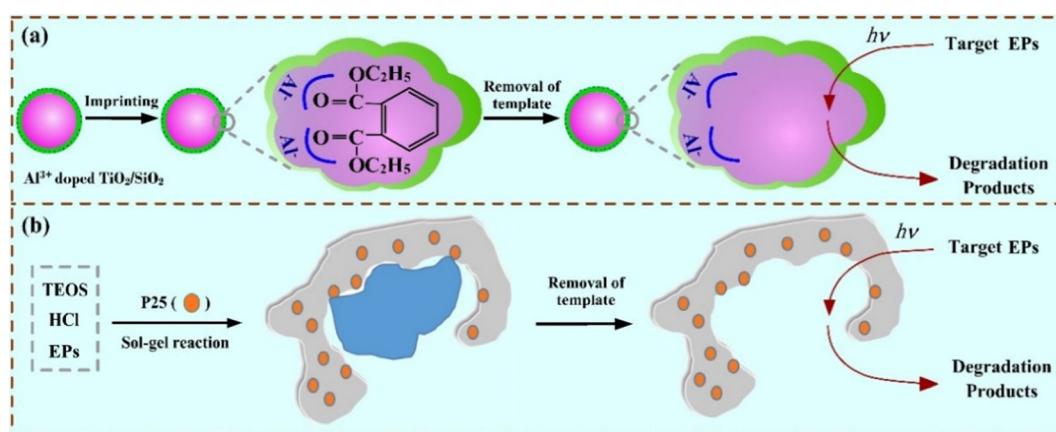
Fig. 3 (a) Schematic route for preparation of inorganic MIP-coated photocatalysts. Adapted with permission from ref. 34. (b) Schematic route for synthesis of MIPCs via an acid-catalyzed sol–gel route. Adapted with permission from ref. 35.
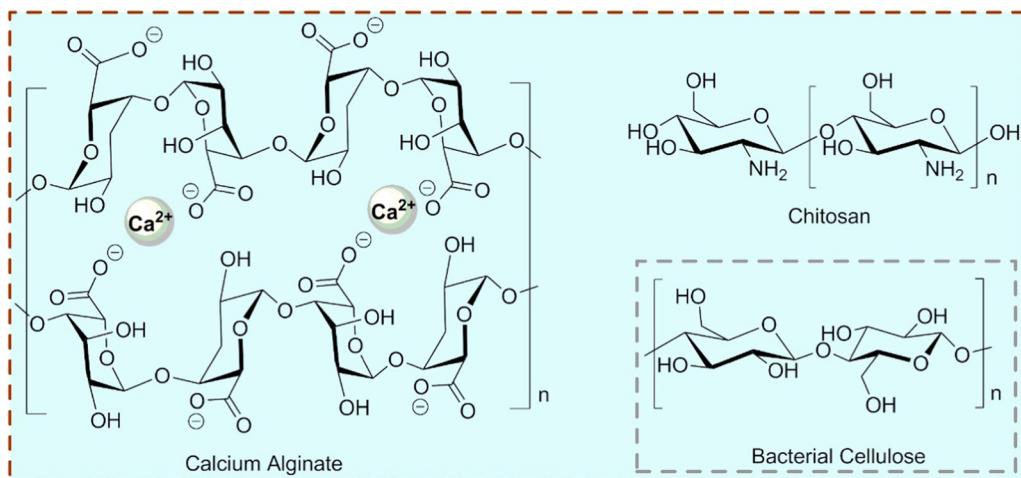
Fig. 4 Structures of the biological hydrogels used in imprinted photocatalysis. The potential biological hydrogel (bacterial cellulose) for synthesis of imprinted photocatalysis is also indicated.

Moreover, to further improve the separation efficiency of the photogenerated electrons and holes, semiconductor nanocomposites containing three components have also been used. A heterostructured MIPC was prepared by using $Bi_2WO_6/CuO/Ag_2O$ as the matrix with a sonochemically assisted sol–gel approach.[60] A Z-scheme imprinted $Ag/Ag_3VO_4/g-C_3N_4$ photocatalyst showed specificity to preferentially remove the target EPs (oxytetracycline and tetracycline), and its selectivity factor was 3.20.[61]

In a word, a single semiconductor and semiconductor nanocomposites containing two or more components could be integrated with molecular imprinting to achieve selective photocatalysis. The general goal for the selection of a suitable photocatalytic matrix is to improve the photocatalytic activity by enhancing the charge separation efficiency. What is more, with the wide development of two-dimensional cocatalysts like the class of MXenes and molybdenum disulfides,[62,63] there are many other alternatives offering emerging modification strategies to improve the photocatalysis of MIPCs based on the construction of different types of heterojunctions.

3.3 Semiconductors doped with non-metal/metal elements

In order to enhance photocatalytic activity under visible light, MIP-coated S-doped TiO_2 nanocomposites were successfully prepared *via* a surface molecular imprinting method using salicylic acid as template molecules.[64] And a boron-doped diamond was used as the substrate to fabricate a n–p heterojunction nanoelectrode with liquid phase deposition (LPD).[65] Besides, other non-metal doped TiO_2 photocatalysts including the Cl-doped,[66] the N-doped,[67] the N–F co-doped[68] photocatalysts were also synthesized.

Recently, to facilitate interfacial charge transfer and limit the electron–hole recombination, metal-doped TiO_2 materials including
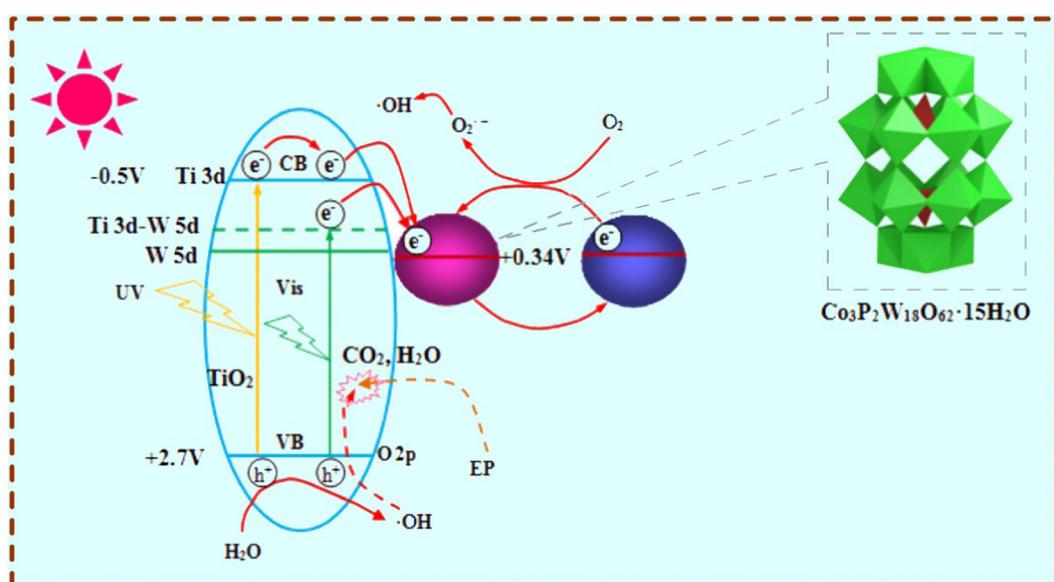
Fig. 5 Schematic mechanism of degradation of the target over the MIPCs. Adapted with permission from ref. 52.

the Ag co-doped, Co-doped or Ag/Zn co-doped nanocomposites[69–71] and the Fe-doped nanofibrous membrane[72] have also been successfully used in the synthesis of MIPCs for visible-light-mediated photocatalysis. Moreover, because the f-orbitals of rare earth elements can contribute to promoting the separation of charge carriers, a Pr-doped molecularly imprinted photocatalyst was fabricated using a facile one-pot solvothermal method.[73] A list summarising the successful dopants used is shown in Fig. 6. For comparison, the most widely used dopants in traditional TiO_2 are also provided. In our opinion, the remaining unreported dopants (highlighted with "*" in Fig. 6) can be also used for the construction of MIPCs.

3.4 Selection of template molecules

In the first report of MIPCs, the target pollutant (4-chlorophenol, 4CP) was directly used as a real template[17] during the synthesis of MIP-coated photocatalysts via surface imprinting in the presence of target molecules and TiO_2 nanoparticles (Fig. 7(a)). These types of MIPCs are named real substrate MIPCs (RS-MIPCs). Due to the great maneuverability, RS-MIPCs have been the most popular catalysts for selective photocatalysis.[74] So far, organic pollutants (including pesticides, antibiotics, endocrine disruptors, dyes, and polycyclic aromatic hydrocarbons), inorganic heavy metal ions, and drugs have been successfully used as real substrate templates for the construction of MIPCs.[21] Recently, some interesting studies on the synthesis of RS-MIPCs has used chiral molecules as the template.[75,76] These studies might open up a new horizon for the RS-MIPCs in chiral pharmaceutical separation on the basis of further studies on the enantioselective degradation of the chiral enantiomers. Apparently, using real templates is a simple and easy method in the preparation of RS-MIPCs. However, some special molecules possess a weak affinity to monomers or low solubility in the polymerization solution, and RS-MIPCs might show a limitation

in practical application. And the leakage of the RS template for the MIPs synthesized with RS templates would affect the detection of target molecules.

To address these problems, pseudo-templates or structural analogues (SA) complementary to substructures of target molecules were commonly used to prepare MIPCs (namely, SA-MIPCs).[77–79] According to the study of the interaction between the functional monomer (o-phenylenediamine, OPDA) and the template molecules (pentachlorophenol, PCP) under the synthesis conditions, an appropriate SA template (4-nitrophenol, 4NP) was selected to prepare the MIPCs (Fig. 7(c)).[77] For example, we used Cr(vi) as the template to synthesize a type of SA-MIPC via Pickering emulsion polymerization by in situ assembling ZnO/GO composites on the synthetic molecular receptors. The obtained SA-MIPCs achieved the selective photoreduction of $[Fe(CN)_6]^{3-}$ since the structure of $[Fe(CN)_6]^{3-}$ was similar to that of Cr(vi).[58]

Besides, because nitrobenzene (NB), halogenated benzene and alkyl benzene lack functional groups for imprinting, they cannot be used as templates to prepare RS-MIPCs or SA-MIPCs. To achieve selective degradation, the synthesis of MIPCs using a transition state analogue (TSA) as the template was reported.[80] In this study, NB was chosen as a model molecule because of its toxicity and slight solubility in water. When an appropriate TSA was selected as the template (mono-nitrophenol), MIP-coated TiO_2 photocatalysts were synthesized by in situ polymerization (Fig. 7(b)). The photocatalytic experiments indicated that the photocatalysts reduced the apparent activation energy and enhanced the photocatalytic degradation of the target NB in both the absence and presence of non-target molecules. Moreover, the special molecular recognition inhibited the accumulation of unwanted intermediates. These results confirmed that using an appropriate TSA of the template to prepare MIP-coated TiO_2 was an efficient way to selectively mineralize the target EPs that cannot be directly used as the template.

Fig. 6 List of the successful dopants used in selective photocatalysis by molecular imprinting.
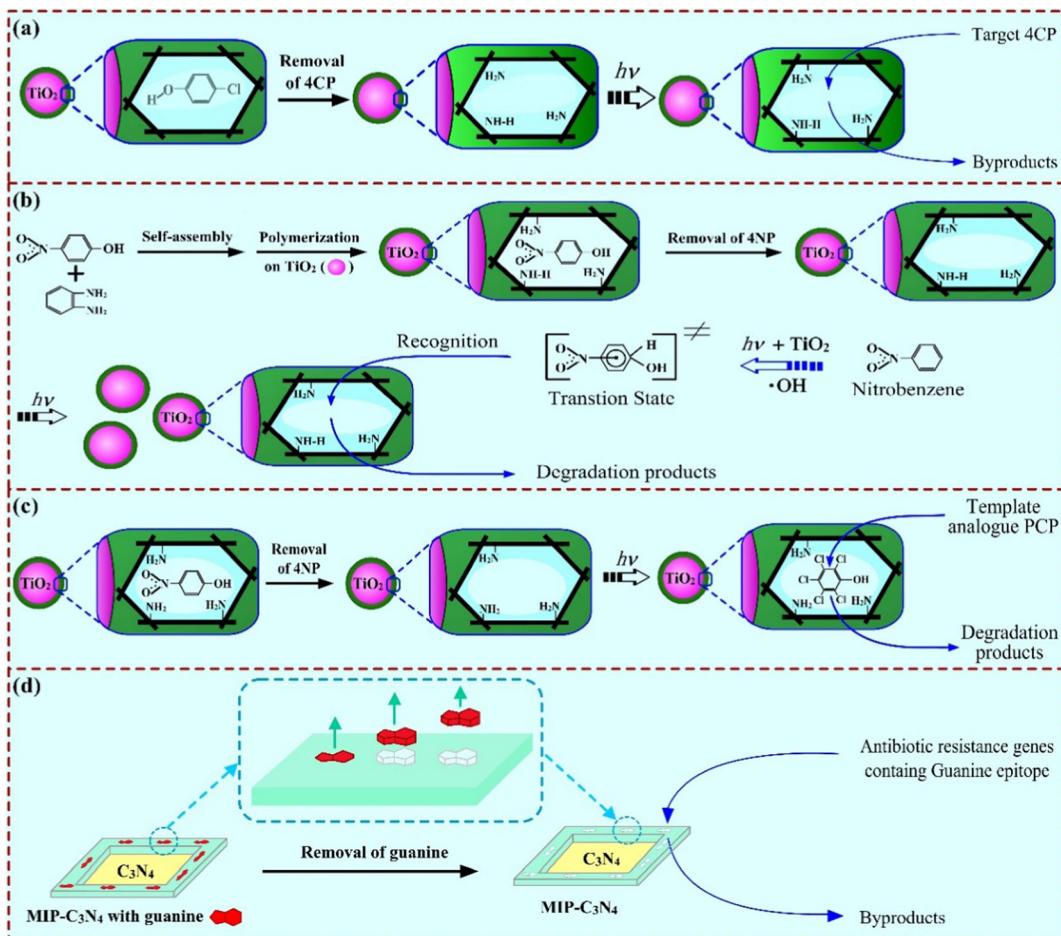
Fig. 7 Schematic route for preparation of (a) RS-MIPCs *via* surface imprinting, adapted with permission from ref. 17; (b) TSA-MIPCs, adapted with permission from ref. 80; (c) SA-MIPCs, adapted with permission from ref. 77, and (d) RS-MIPCs by using an epitope imprinting method, adapted with permission from ref. 81.

What is more, if the targets are biomacromolecules, the traditional MIPs synthesized with RS templates would make the removal of the template and the rebinding of the target difficult. In this case, epitope templates, which are unique combinations of amino acid (or gene base) sequences positioned on exposed domains of proteins (or DNA), are always selected as the templates for the synthesis of biomacromolecule-imprinted polymers. Recently, by using an epitope imprinting method, guanine-imprinted photocatalysts were synthesized (Fig. 7(d)).[81] The obtained MIPCs displayed a photocatalytic degradation rate constant of 0.111 min^{-1} towards the target (antibiotic resistance genes, ARGs), which was 1.7 times and 37 times higher than that on the neat P25 and C$_3$N$_4$, respectively. We believe that this method will be a common method for selective removal of macromolecular pollutants beyond ARGs, including harmful peptides, proteins and bacteria. Moreover, this method also shows great potential for the selective removal of drug-resistant bacteria or tumor cells in biomedicine.

3.5 Selection of monomers and cross-linkers

In accordance with traditional systems for the synthesis of MIPCs, different types of monomers and cross-linkers, such as acrylic acid (AA), methacrylic acid (MAA), acrylamide (AM), 4-vinyl pyridine (4-VP), *N*-isopropyl acrylamide (NIPAM), ethylene glycol dimethacrylate (EGDMA), methylenebisacrylamide (MBAA), trimethylolpropane trimethylacrylate (TRIM), divinylbenzene (DVB) and *N,N'*-methylenebis-acrylamide (BIS), were most commonly used to prepare hydrophobic/hydrophilic MIPs, and these MIPs formed a non-conductive layer on the surface of semiconductors. Although MAA was somehow hydrophilic, poly(EGDMA-MAA) or poly(TRIM-MAA) was hydrophobic and decreased the degradation selectivity in water.[82,83] Recently, the MIPCs were prepared by using AM and NIPAM as functional monomers respectively, which showed the same high adsorption capacity and photocatalytic selectivity.[84,85] Besides both hydrophilic monomers and hydrophilic cross-linkers being used to generate MIPCs, selective removal of EPs in a mixture wastewater system was also achieved by using molecularly imprinted poly(MAA-BIS).[86] AM and NIPAM might be much more suitable as monomers for the synthesis of MIPCs than MAA, and further introduction of hydrophilic cross-linkers will enhance the water compatibility of MIPCs.

What is more, using conductive monomers to form a heterojunction structure with semiconductors should be taken into consideration. At first, pyrrole is the most famous candidate

of these monomers. The Nobel Prize in Chemistry was awarded in 2000 for the work on conductive polymers including poly-pyrrole (PPy) formed by polymerization of pyrrole. Generally, the PPy/semiconductor composites showed much better photo-catalytic activity than the pure semiconductor photocatalysts.[87] So far, several MIPCs have been fabricated using PPy as the functional monomer (like the PPy/TiO$_2$ and ZnFe$_2$O$_4$/PPy photocatalysts).[88,89] Besides, the class of phenylenediamine is another commonly used monomer. For example, TiO$_2$/CNDs/MIP photocatalysts displayed a high binding capacity of 86.1 mg g^{-1} in 30 min and enhanced selectivity, which were synthesized by using OPDA by the means of the surface molecular imprinting.[90] And the poly(p-phenylenediamine) (PPPDA) TiO$_2$ nanocomposites were synthesized by using p-phenylenediamine (PPDA) as the functional monomer and salicylic acid as the template molecule, which enhanced the visible absorption edge and showed higher adsorption capacity for salicylic acid compared to the naked TiO$_2$ nanoparticles.[64] Also, poly-3,4-ethylenedioxythiophene (PEDOT) was reported as the functional monomer to prepare molecularly imprinted heterojunction photocatalysts, which could harvest the visible light.[91]

In summary, the structure of conductive polymers reported for MIPCs is provided in Fig. 8. To better understand the gap between MIPCs and the traditional MIPs, other conductive polymers that are used in conventional MIPs but not used for the construction of MIPCs are also shown, such as polythio-phene (PTh) and polyaniline (PAn). As an efficient electron donor under visible light, in the future, the conductive polymers and their derivatives could be widely introduced in the synthesis of MIPCs. The possible photocatalytic mechanism of the conduc-tive polymer-based MIPCs has been investigated using X-ray photoelectron spectroscopy (XPS), Fourier transform infrared (FTIR) spectroscopy and electron spin resonance (ESR) spectro-scopy. Indeed, their photocatalytic mechanism is yet not clear and more studies should be contributed in this field.

3.6 Consideration of other functional materials

At present, some new functions have also been incorporated into MIPCs, which made them more efficient. First, in order to recycle the photocatalysts for secondary utilization, many studies reported that magnetic materials can be introduced into the synthesis of MIPCs forming a magnetic-TiO$_2$ core and a MIP shell.[20,92] For example, by using a mild sol–gel method assisted with microwave heating, a magnetically imprinted TiO$_2$ photo-catalyst with an imprinted poly(MAA-TRIM) shell and a magnetic TiO$_2$@SiO$_2$@Fe$_3$O$_4$ core was synthesized.[93] The magnetically imprinted photocatalyst exhibited a higher photocatalytic effi-ciency in comparison with the control photocatalysts, and the apparent rate constant (k) for degradation was 1.08 min^{-1}. Interestingly, Zhang et $al.$ reported that the introduction of an inter Al$_2$O$_3$ layer could enhance the photocatalytic activity of the Fe$_3$O$_4$/Al$_2$O$_3$/molecularly imprinted TiO$_2$ photocatalyst compared to the Fe$_3$O$_4$/molecularly imprinted TiO$_2$ nanocomposites.[94]

Generally, a photocatalytic reaction is hard to be controlled under complex conditions, but it is associated with a temperature change. To achieve the regulation by changing the reaction temperature, the fabrication of thermal-responsive MIPCs attracted a lot of attention.[95,96] For example, using NIPAM and EGDMA as monomers, thermo-responsive molecularly imprinted polymers (TMIPs) for selective photodegradation of sulfadiazine (SD) were prepared via surface-initiated reversible addition frag-mentation chain transfer (SI-RAFT) polymerization.[95] The TMIPs showed an outstanding specific affinity and high degradation activity toward target SD. Due to the thermo-responsiveness of poly-NIPAM shells, the photocatalytic activity of the TMIPs could be controlled by the environmental temperature.

As porous materials, moreover, metal–organic frameworks (MOFs) have attracted increasing attention because of their merits such as controllable pores and open metal active sites.[97] Although the common MOFs always lack poor binding selectivity, we recently produced imprinted MOFs with specific recognition defects by integrating molecular imprinting and MOF generation.[98] A schematic illustration of selective photocatalysis of the target on the imprinted MOFs is shown in Fig. 9(a). The morphologies of the resulting non-imprinted MOFs (Fig. 9(b)) and the imprinted MOFs (Fig. 9(c)) were observed using a SEM. The imprinted cavities within the MOFs could act as both high-affinity binding cavities and active defects for photocatalysis. The pseudo-first-order kinetic curves for degradation of the target over imprinted MOFs and non-imprinted MOFs are shown in Fig. 9(d) and (e), respectively. Compared to the non-imprinted MIL-101_NH$_2$ system, the imprinted MIL-101_NH$_2$ system showed a much higher photocatalytic activity (64%) with a photocatalytic selectivity of 4.74. According to the intermediate analysis at
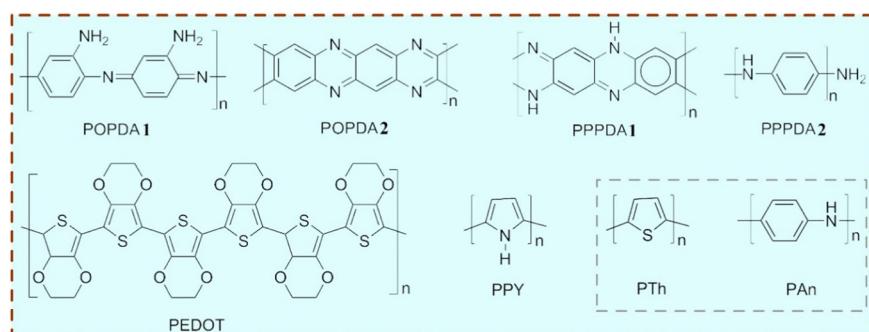

Fig. 8 Conductive polymers used for synthesis of MIPCs. The inserted polymers have been only used in conventional MIPs.
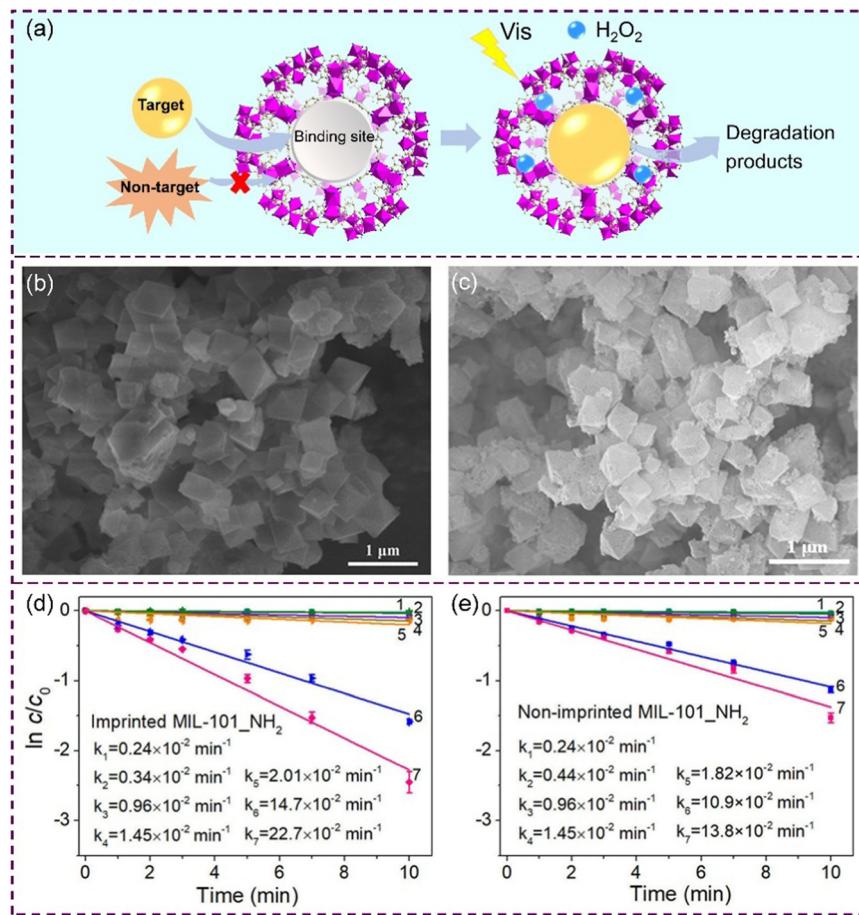
Fig. 9 (a) Schematic illustration of selective photocatalysis of the target on imprinted MOFs. (b) SEM image of the non-imprinted MOFs. (c) SEM image of the imprinted MOFs. The pseudo-first-order kinetic curves for degradation of the target over (d) imprinted MOFs and (e) non-imprinted MOFs. Adapted with permission from ref. 98.

different reaction times (Fig. 10(a)) and the possible degradation pathway of sulfadimidine (SM2) on the imprinted MIL-101_NH$_2$ system (Fig. 10(b)), the cleavages of the N–S bond (δ position), C–S bond (γ position) and C–N bond (ε position) were the main pathways for the target SM2 degradation on the imprinted MOFs.

In short, besides the above materials, hydroxyapatite[99] and magnetic fly ash[100,101] have been employed as photocatalytic substrates to synthesize MIPCs as well. These studies show that metal-doped phosphorus aluminum molecular sieves, noble metal complex photocatalysts, non-noble metal complex photocatalysts and single-metal atom photocatalysts have great potential and might also be used for preparing MIPCs, and the synthesis of these MIPCs could promote another hot topic in the field of selective photocatalysis.

3.7 Validation of the photocatalytic mechanism by characterization and DFT calculations

There is a definite need to explore the photocatalytic mechanism of newly prepared MIPCs. In general, for the study of photocatalytic active sites, some characterization approaches have been chosen to characterize the morphology, the surface groups, and photoelectrochemical properties, such as SEM, FT-IR spectroscopy, XRD, and XPS spectral analysis. As shown in

Fig. 11, for example, to compare the different characters of the materials synthesized by typical hydrothermal synthesis (HTS) and LPD, the abovementioned characterization methods were applied, which resulted in clear distinctions in the construction strategy and chemical groups on the surface.[75] In particular, to further explore the crystal structure and confirm the properties, TEM analysis and Raman spectroscopy were employed. Indeed, these techniques synergistically assist in the validation but were not obligatory. Otherwise, the density functional calculation (DFT) is an effective method to reveal the exact catalytic mechanism as well. For instance, to prove that functional groups on the surface of imprinted alginate beads (called IUA) could impact the adsorption–photoreduction of the ion (Au(III)), a spin-polarized-based DFT calculation was perfomed *via* the DMol3 program module.[102] And, binding energy (E_b), an important parameter, was successfully obtained according to eqn (10) as follows:

$$E_b = E(\text{complex}) - E(\text{IUA}) - E(\text{AuCl}_4^-) \qquad (10)$$

where $E(\text{complex})$ is the energy of the complex, $E(\text{IUA})$ is the energy of the IUA adsorbent with one negative charge, and $E(\text{AuCl}_4^-)$ is the energy of AuCl_4^-. And by combining the results of the partial density of states, it was found that S had a higher activity and its interaction with Au exhibited a more negative
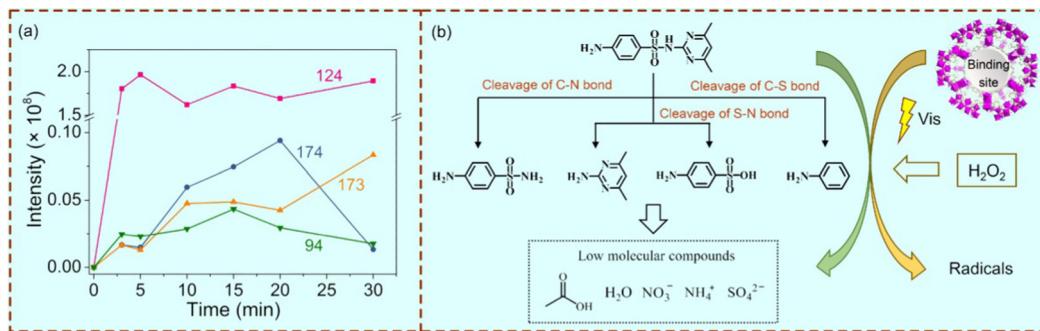
Fig. 10 (a) UPLC-MS intensity changes of the intermediate products at different reaction times during the photodegradation of SM2 over imprinted MIL-101_NH$_2$. (b) Proposed SM2 degradation pathways over the imprinted MIL-101_NH$_2$. Adapted with permission from ref. 98.

binding energy, indicating that the stability of the S–Au bond was better than that of the O–Au bond, which was similar to the outcomes of the FT-IR and XPS spectra. This study provides a good idea for the study of the mechanism related to metal photoreduction and could promote the theoretical validation into sights.

4. Application of molecularly imprinted photocatalysts

With the development of selective photocatalysis in the past few decades, kinds of MIPCs have been synthesized and applied to solve environmental problems. Under different light

irradiation conditions, target molecules have a selective affinity for these MIPCs and are removed by oxidation or reduction. Besides, because of the electrochemical-response ability and specific recognition of some MIPCs and inspired by selective photocatalytic degradation, a few photoelectrochemical sensors based on imprinted semiconductors were fabricated for suppressing background noise interference in detection recently.

4.1 Selective degradation of target molecules with a photooxidation system

At the beginning of the application of photocatalysis in the degradation of EPs, it mainly targets all kinds of industrial pollutants, most of which are organic molecules that are difficult to biodegrade. According to the principle of conventional
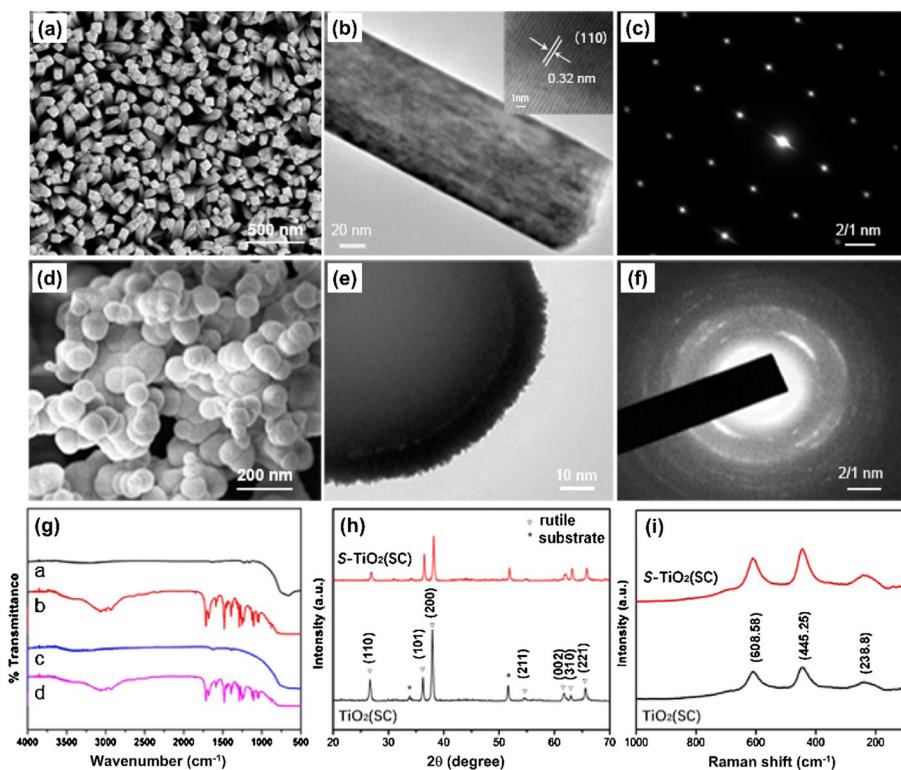

Fig. 11 (a), (d) FE-SEM images, (b), (e) TEM images, (insets: the corresponding HRTEM images), and (c), (f) SAED patterns of S-TiO$_2$ (HTS) and S-TiO$_2$ (LPD), respectively. (G) FTIR spectra of S-TiO$_2$, (h) XRD and (i) Raman spectra of TiO$_2$ (SC) and S-TiO$_2$ (SC). Adapted with permission from ref. 75.

photocatalytic degradation mentioned above and the trait of organics, a photooxidation system is often the first choice. Therefore, for the selective degradation of common highly toxic organics, the high adsorption and oxidation efficiency of MIPCs is an important criterion. Based on literature research and a summary from recently published reviews,[21–23] it is not difficult to find that many MIPCs have been synthesized with surface imprinting for the oxidative degradation of diethyl phthalate and nitrophenol. Similarly, some derivative methods based on the photooxidation system were also reported in the field of refractory organics removal, such as the molecular imprinting assisted Fenton process and persulfate (PS) catalytic decomposition.[103,104] Table 1 summarizes the reported studies on degradation performance with these derivative systems. Accordingly, more kinds of iron-containing heterogeneous imprinted catalysts were synthesized for the efficient removal of phthalates by PS catalytic decomposition.[113–117]

In addition, paying more attention to the persistent human hazards of pesticides and the abuse of antibiotics, some MIPCs were successfully prepared to enhance photodegradation specificity for the removal of these health-related substances. Taking photocatalytic removal of danofloxacin mesylate (DM) as an example, Lu *et al.* synthesized a magnetically imprinted PEDOT/CdS photocatalyst by microwave-assisted surface imprinting.[44] The transient photocurrent and Nyquist plots of different prepared materials are shown in Fig. 12(a) and (b). The photodegradation of the target over different materials under visible light irradiation is shown in Fig. 12(c). It is seen that, compared to the non-imprinted PEDOT/CdS photocatalyst, the imprinted PEDOT/CdS photocatalyst showed a degradation selectivity coefficient of 2.11 towards the target. The possible photocatalytic reaction mechanism of this photocatalyst was investigated (Fig. 12(d)). Because of the negative energy level of the imprinted photocatalyst, photogenerated e^- would form $^\bullet O_2^-$ and $^\bullet OH$. The target was then oxidized into the corresponding byproducts by the photoexcited h^+ as well as the produced $^\bullet O_2^-$ and $^\bullet OH$ under visible light. The reusability of the magnetically imprinted photocatalyst indicated that the PEDOT imprinted layer still had excellent photocatalytic performance and reproducibility after 5 cycles (Fig. 12(e)). Moreover, to photodegrade the endocrine disrupting chemicals (bisphenol A and BPA), the imprinted poly(EGDMA-MAA) coated sulfur-doped nano-titanium dioxide was reported.[82] A schematic of the degradation process, the SEM analysis, and the binding profiles of this photocatalyst are shown in Fig. 13.

4.2 Selective removal of metal ions with a photoreduction system

As is known, high-valence heavy metal ions are generally more harmful to the body, so the photoreduction reaction is much helpful for the removal of heavy metal ions. So far, selective photoreduction of Ag^+, $Au(III)$, Cu^{2+} and $Cr(VI)$ by MIPCs has been achieved in different studies.[102,118–120] For example, by using alginate as a monomer and calcium as a cross-linker, $Au(III)$ imprinted porous epichlorohydrin/thiourea modified alginate beads were synthesized.[102] The imprinted adsorbent displayed outstanding binding selectivity towards the target $Au(III)$ from multi-metallic solutions with a binding capacity of 184.82 mg g^{-1}. Interestingly, photoreduction of $Au(III)$ to gold particles might occur during the binding process under UV light illumination. The schematic illustration of the optimized binding configuration of $AuCl_4^-$, thiol groups with $AuCl_4^-$, and carboxyl groups with $AuCl_4^-$ is shown in Fig. 14(a)–(c), respectively. Similarly, selective reduction of Cu^{2+} with an ion imprinted POPD-CoFe$_2$O$_4$ heterojunction photocatalyst has also been successfully reported.[49] The proposed selective reduction mechanism of Cu^{2+} on the magnetic ion-imprinted heterojunction photocatalyst is shown in Fig. 14(d). The reduction selectivity coefficient of the magnetic ion-imprinted heterojunction photocatalyst relative to the control materials reached a value of 4.998.

Table 1 Degradation performance with the molecular imprinting-assisted Fenton process and persulfate catalytic decomposition

Target	Catalytic structure	Catalytic substrate	Monomer/cross-linker	Chemical dose	Degradation performance	Ref.
Norfloxacin	Core–shell	γ-Fe$_2$O$_3$	Chitosan/glutaraldehyde	0.03 mM[a]	$k = 0.0012$ min^{-1}	105
Ribavirin	Membrane	γ-Fe$_2$O$_3$	MAA, AM/DMPA[c]	0.05 mM[a]	Removal capacity $\approx$ 25 mg g^{-1}	106
Dimethyl phthalate	Iron-doped carbon	Activated iron	Carbon aerogel	50 mg L^{-1}[a]	Removal = 98%	107
Acid orange II	Composite	Fe-doped TiO$_2$	TiO$_2$	0.04 mM[a]	$k = 0.5861$ min^{-1}	108
Methylene blue	Fe-zeolites	Fe-zeolites	Zeolites	25 g L^{-1}[a]	Removal = 87.7%	103
Methyl orange	Bulk	Fe(II)-complex	EDMA/MBAA	2.93 mM[a]	Removal = 95.7%	109
Cr(VI)	Core–shell	Fe(III)-complex	4-VP/EGDMA, TRIM	3 mg L^{-1}[a]	Removal = 66.0%	110
Sulfamethoxazole	Core–shell	NH$_2$-MIL-53	AA/DVB	791 μL mL^{-1}[a]	Removal $\approx$ 48%	111
Sulfamethoxazole	Core–shell	NH$_2$-MIL-53	AA/DVB	1.88 g L^{-1}[b]	Removal $\approx$ 90%	111
Sulfadimidine	MOFs	MIL-101_NH$_2$	MIL-101_NH$_2$	10 mM[b]	$k = 0.227$ min^{-1}	98
Tetrabromobisphenol A	Core–shell	C–Fe–Nx	MAA/DVB	0.9 g L^{-1}[b]	Removal capacity = 104.6 mg g^{-1}	112
Diethyl phthalate	Core–shell	MIL100(Fe)	MAA/EGDMA	3 g L^{-1}[b]	Removal capacity = 13.6 mg g^{-1}	104
Diethyl phthalate	Core–shell	MIL100(Fe)	AA/DVB	14 g L^{-1}[b]	$k = 0.59$ h^{-1}	113
Diethyl phthalate	Core–shell	C-MIL-100	AA, AM, MAA/DVB	0.5 g L^{-1}[b]	Removal capacity = 1.68 mg g^{-1}	114
Dimethyl phthalate	Core–shell	C-MIL-100	AA, AM, MAA/DVB	0.5 g L^{-1}[b]	Removal capacity = 3.93 mg g^{-1}	114
Dimethyl phthalate	Core–shell	Fe-MOF-74	MAA/EGDMA	26 mM[b]	Removal $\approx$ 98%	115
Dimethyl phthalate	Core–shell	Fe-MOF-74	MAA/EGDMA	30 mg L^{-1}[b]	$k = 0.003$ min^{-1}	116
Dibutyl phthalate	Core–shell	Fe(II)-MOFs	MAA/EGDMA	0.7 g L^{-1}[b]	$k = 0.071$ min^{-1}	117

[a] $[H_2O_2]_0$. [b] $[PS]_0$. [c] 2,2-dimethoxy-2-phenylacetophe-none.
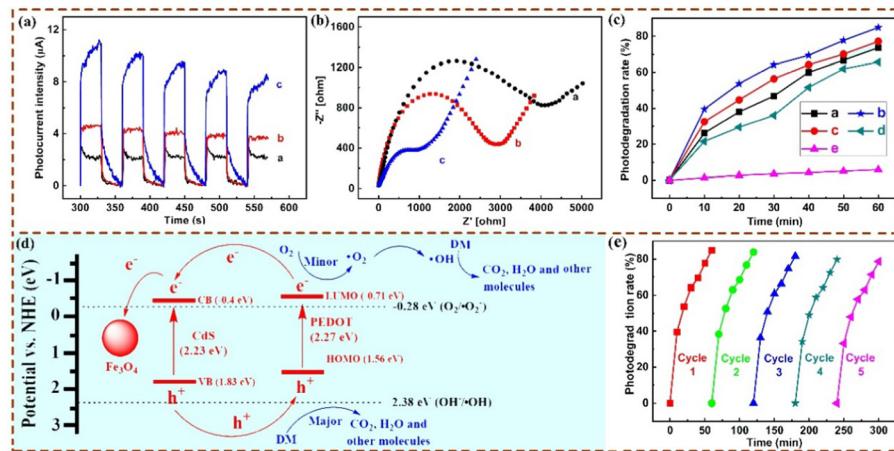
Fig. 12 (a) Transient photocurrent and (b) Nyquist plots of electrochemical impedance spectroscopy (EIS) for different materials. (c) Photodegradation of DM over different catalysts under visible light irradiation. (d) Energy level positions of CdS and PEDOT and schematic diagram for photoexcited electron–hole separation processes in the magnetic imprinted photoreactor. (e) Reusability of the magnetic imprinted photocatalysts. Adapted with permission from ref. 44.

Besides the cations used as templates, anions also were used as the template. For instance, He *et al.* used $Cr_2O_7^-$ to produce uniform ion-imprinted $ZnFe_2O_4$ particles.[50] The reduction rate of Cr(VI) to Cr(III) was 92.67%. The possible photoreduction mechanism of Cr(VI) reduction on the imprinted $ZnFe_2O_4$ is shown in Fig. 14(e). On this catalyst, the target Cr(VI) could be directly reduced by the excited electrons. Moreover, for selective Cr(VI) reduction, another imprinted photocatalyst was prepared *via* Pickering emulsion polymerization by *in situ* assembling ZnO/GO composites on the MIPs.[58] The photoluminescence (PL) spectra, plots of the transformed Kubelka–Munk function *versus* light energy, valence band XPS spectra of ZnO and ZnO/GO and the schematic illustrations of energy levels for GO, ZnO and ZnO/GO are presented in Fig. 15. The experimental data
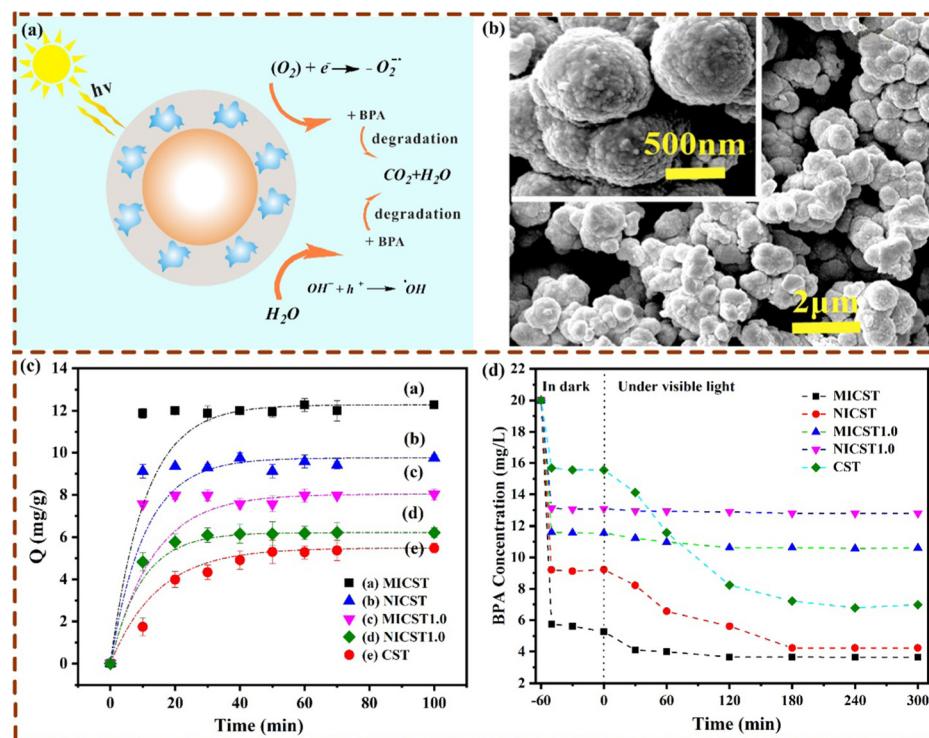

Fig. 13 (a) Schematic representation of the target HTP photodegradation on the imprinted photocatalysts, (b) SEM image of the imprinted photocatalysts, (c) adsorption kinetics of HTP on the imprinted and the control photocatalysts, and (d) concentration of HTP in the dark and under visible light illumination. Adapted with permission from ref. 82.
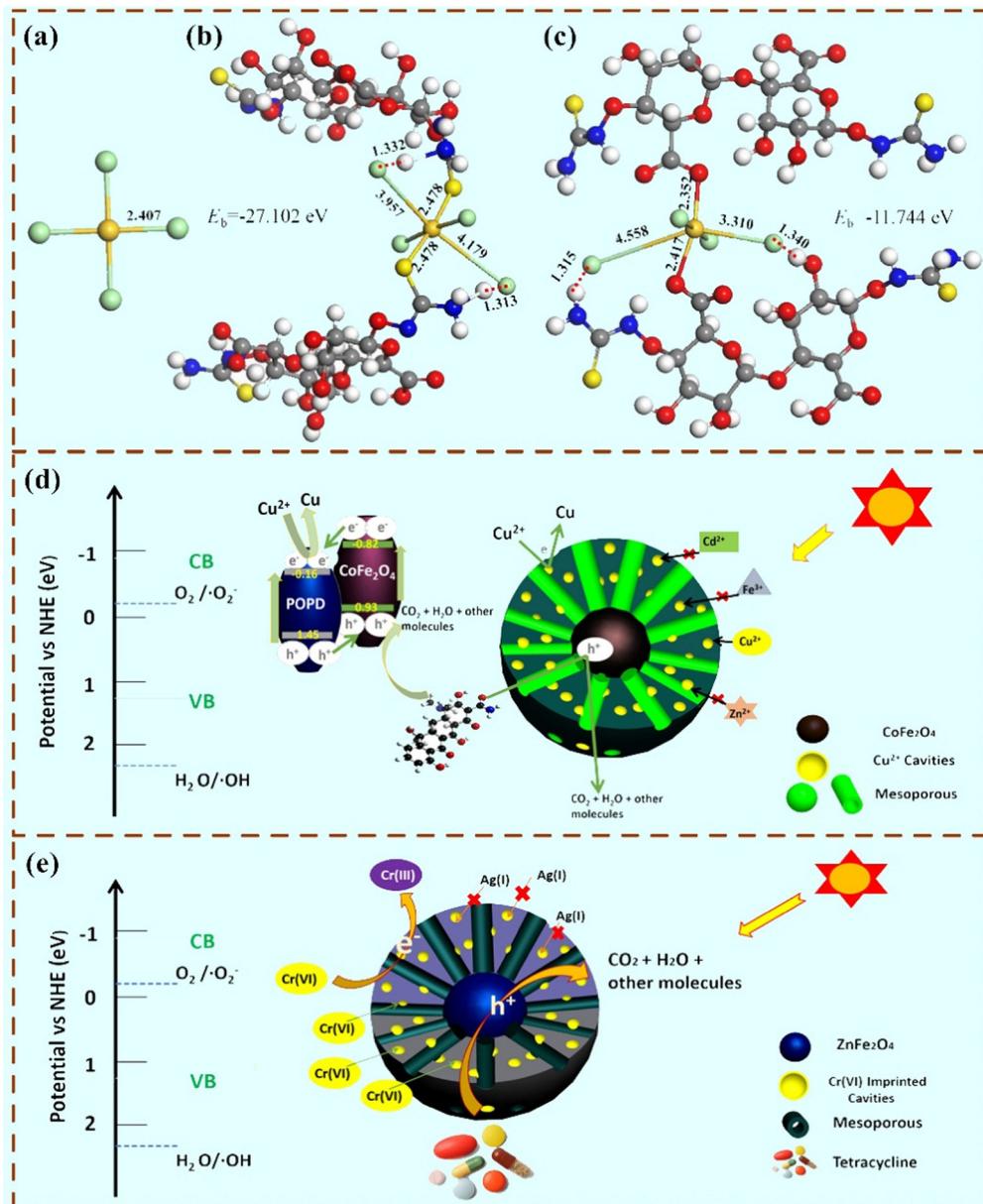
Fig. 14 Schematic illustration of the optimized binding configuration of (a) $AuCl_4^-$, (b) thiol group with $AuCl_4^-$, and (c) carboxyl group with $AuCl_4^-$. Adapted with permission from ref. 102. (d) Proposed selective reduction mechanism of Cu^{2+} on the magnetic ion imprinted heterojunction photocatalyst. Adapted with permission from ref. 50. (e) Possible photoreduction mechanism of Cr(VI) reduction on the imprinted $ZnFe_2O_4$. Adapted with permission from ref. 49.

indicated that the existence of Cr(VI) imprinted cavities promoted the reduction selectivity of Cr(VI) during photocatalysis.

4.3 Fabrication of photoelectrochemical sensors for enhancing detection selectivity

Before efficiently removing EPs, target monitoring is the first step. In particular, influenced by the global spread of COVID-19, the detection of biogenic substances has attracted more attention of not only scientists but also ordinary people. Various techniques are available in laboratories, such as PCR, ELISA, ICP-MS, etc., but these methods are usually not suitable for rapid detection in the home or community because of the complex pretreatment and more analytical time.[121] And nowadays, electrochemistry-based analytical methods, such as the photoelectrochemical, have been vigorously developed in the field of rapid detection and diagnosis due to its high sensitivity, simple operation, rapid response, and easy online monitoring.[122] To overcome the limitation of traditional photoelectrochemical sensors of the lack of selectivity, many photoelectrochemical sensors based on MIPs have been fabricated and exhibited a favorable performance towards the detection of the targets.[123] Inspired by selective photocatalytic degradation, recently, several studies reported that a few molecularly imprinted semiconductors with electrochemical-response ability showed great potential in

the fabrication of photoelectrochemical sensors for enhancing detection selectivity.[124–127] A schematic diagram of photoelectrochemical sensors based on MIPCs is shown in Fig. 16. For example, imprinted TiO₂ coated multi-walled carbon nanotubes (MI-TiO₂@CNTs) were successfully used to establish a sensor toward microcystin-LR. Using this sensor, the determination of targets was possible in a wide linear range from 1.0 pM to 3.0 nM with a high photocurrent response sensitivity, even though under 100-fold potential co-existing interferences.[128]

Table 2 summarizes the reported studies on photoelectrochemical sensors by using molecularly imprinted semiconductors. Interestingly, for suppressing background noise interference in high sensitivity surface-enhanced Raman scattering detection, a sandwiched silver microsphere/TiO₂ nanoparticles/molecular imprinted polymer was synthesized to decompose residual templates by photocatalytic degradation,[137] and used it in the detection of sulfamethazine with a minimum detection concentration of 3.6 nM. In a word, we believe that diversity of applications based on selective photocatalysis by molecular imprinting is coming soon.

Challenges and outlook

Molecular imprinting provides interesting potential for selective removal of EPs at low concentrations in the presence of less harmful pollutants at high concentrations. In this field, selective photodegradation of EPs based on MIPCs has improved dramatically over the past few years. This review discussed the basic principles of molecular imprinting and selective photocatalysis. The comprehensive design and synthesis routes of MIPCs related to real performance are reviewed. We also summarized various applications of selective photocatalysis by molecular imprinting, such as selective photocatalytic removal of organics, antibiotics, and metal ions based on conventional oxidation, reduction, or derivation systems, and especially highlighted the fabrication of photoelectrochemical sensors for enhancing detection selectivity.

Despite a lot of achievements made so far, there are still some potential challenges to be overcome and efforts that should be made by researchers: (i) in reality, there are always several EPs that co-exist with industrial emissions, but only the removal of a single pollutant in the spiked system was reported in most publications. Therefore, more efforts should be made on photocatalytic degradation of mixed EPs in a practical system. Using mixed EPs to highlight the potential of MIPCs for the removal of multiple EPs coexisting in real samples may be a smart selection. Moreover, a better understanding of the simultaneous decomposition of mixtures might be helpful for the design of MIPCs with high efficiency. (ii) At present, using a real substrate template, a structural analogue of a template, an epitope template, or a transition state analogue of a template is a series of effective but common methods in the synthesis of MIPCs. Recently, two preparation approaches using hydroxyl groups or multiple templates containing both sugar (with plenty of hydroxyl groups) and target molecules that produce highly effective photocatalysts have been reported, but the utilization efficiency of peroxides by target molecules should be carefully investigated. (iii) MIPCs with an organic MIP layer and a semiconductor shell may enhance the photodegradation selectivity. However, the organic MIP layers including the conductive MIP layer will be decomposed under UV illumination for a long duration. Using the inorganic SiO₂ MIP layer could increase the lifetime of the MIP layer, but the presence of SiO₂ decreases the utilization efficiency of light. Therefore, full
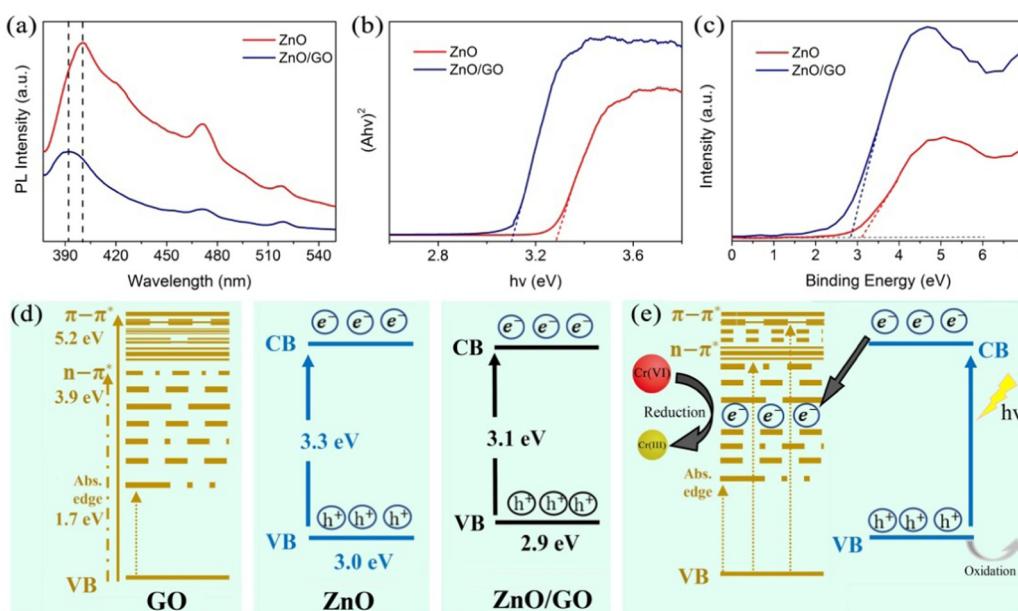
Fig. 15 (a) Photoluminescence (PL) spectra of ZnO and ZnO/GO. The excitation wavelength was 350 nm. (b) Plots of transformed the Kubelka–Munk function versus light energy for ZnO and ZnO/GO. (c) Valence bands (VB) XPS spectra of ZnO and ZnO/GO. (d) Schematic illustrations of energy levels for GO, ZnO, and ZnO/GO. (e) Possible photoreduction mechanism of Cr(ʋɪ) on the photocatalysts. Adapted with permission from ref. 58.
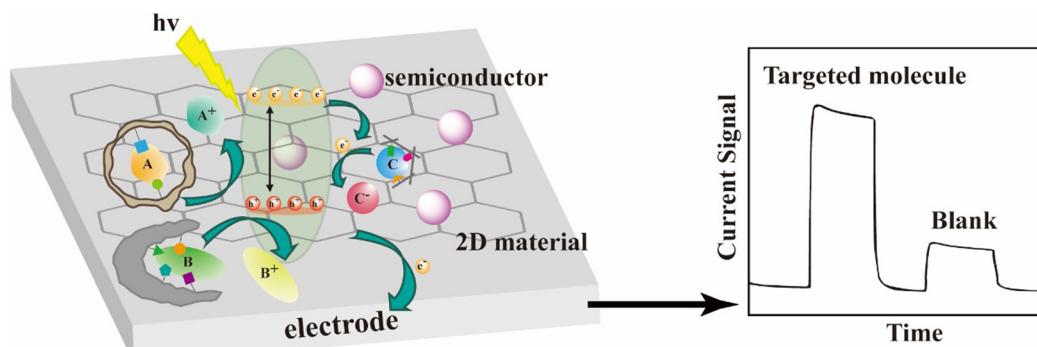
Fig. 16 Schematic diagram of photoelectrochemical sensors based on MIPCs.

Table 2 Photoelectrochemical sensors by using molecularly imprinted semiconductors

Detection target	Semiconductor	Linear range	Detection limit	Light source	Ref.
Uric acid	TiO_2	0.3–34 μM	0.02 μM	UV	124
Atrazine	TiO_2	0.12–93 μM	8 nM	UV	125
Bilirubin	TiO_2	0.03–28 μM	1 nM	UV	126
Glycoprotein (RNase B)	TiO_2	0.5 pM–2 μM	0.12 pM	UV	127
Microcystin-LR	TiO_2	1.0 pM–3.0 nM	0.4 pM	Visible light	128
Microcystin-LR	Cu_2O	1.0–100 ng L^{-1}/0.1–10 μg L^{-1}	0.23 ng L^{-1}	Visible light	129
Pentachlorobiphenyl	TiO_2	0.1 pM–0.5 nM	0.05 pM	UV	130
Dichlorophenoxyacetic acid	Sn_3O_4	0.05–100 nM	10.8 pM	Visible light	131
L-Glutamic acid	ZnO	20 pM–1 μM	9.6 pM	UV	132
L-Cysteine	ZnO	50 pM–800 nM	24 pM	UV	132
Progastrin-releasing peptide	MoS_2	0.02–5 ng mL^{-1}	3.2 ng L^{-1}	White light	133
L-Phenylalanine	CdS/CdSe	0.005–2.5 μM/2.5–130 μM	0.9 nM	Visible light	134
Bilirubin	$g\text{-}C_3N_4$	1.0–200 pM	0.1 pM	Visible light	135
Bisphenol A	TiO_2	0.05–5.00 μM/5.00–50.00 μM	0.03 μM	Visible light	136

consideration is needed in the selection of monomers, and the direct creation of imprinted cavities in semiconductor photocatalysts will attract more attention. (iv) MIPCs generally have semiconductors as the photocatalytic core. In the future, non-semiconductor materials including photosensitizers, metal–organic frameworks, hydroxyapatites, metal-doped phosphorus aluminum molecular sieves, noble metal complex photocatalysts, non-noble metal complex photocatalysts and single metal atom photocatalysts might also be used to fabricate novel MIPCs. The synthesis of these photocatalysts will be another hot topic in the field of selective photocatalysis. (v) Although lots of efforts have been made to understand the photodegradation mechanism of the target molecules on the imprinted semiconductor nanocomposites, the differences between the normal semiconductor nanocomposites and the imprinted semiconductor nanocomposites have never been considered. The possible photocatalytic mechanism of the imprinted photocatalysts was investigated using XPS spectroscopy, FTIR spectroscopy and ESR spectroscopy. More *in situ* or online characterization studies, including *in situ* FTIR/DRIFTS, synchrotron radiation, LC-MS and PTRTOF-MS, are suggested for the investigation of the degradation mechanisms. Also, they might help researchers to understand the migration and transformation of target molecules and their intermediate species during the photodegradation process, and thus the degradation

pathways of the EPs restricted in the imprinted cavities would be revealed. (vi) The robustness of MIPCs should attract more attention because of the complex photocatalytic reaction environments in the practical application. Until now, most MIPCs were synthesized with the aim of overcoming environmental problems, however poor stability of their imprinted sites and total structure could prevent their reuse. Hence, it is necessary to carefully select a design combination from the key factors or evolutionarily develop new methods.

In this review, we provide comprehensive guidance for the preparation of common MIPCs and some outlooks on innovative applications of selective photocatalysis by molecular imprinting for the design of novel MIPCs. With the progress of molecular imprinting and materials science, there is no doubt that more MIP-based photocatalysts with high specific adsorption capacity and photocatalytic activity will be developed for targeted monitoring and removal of environmental pollutants in the future.

Author contributions

Yaoyu Luo and Xinrui Feng contributed equally: conceptualization, writing-draft, visualization, investigation, reviewing, and editing; Zhiliang Chen: investigation and writing-reviewing and

supervision; and Xiantao Shen: conceptualization, funding acquisition, and writing-reviewing and editing.

Conflicts of interest

There are no conflicts to declare.

Acknowledgements

References

1 A. Fujishima and K. Honda, *Nature*, 1972, **238**, 37–38.
2 F. P. García de Arquer, D. B. Talapin, V. I. Klimov, Y. Arakawa, M. Bayer and E. H. Sargent, *Science*, 2021, **373**, eaaz854.
3 A. Kumar, P. Choudhary, A. Kumar, P. H. C. Camargo and V. Krishnan, *Small*, 2022, **18**, 2101638.
4 V. Kurnaravel, S. Mathew, J. Bartlett and S. C. Pillai, *Appl. Catal., B*, 2019, **244**, 1021–1064.
5 C. Xu, P. Ravi Anusuyadevi, C. Aymonier, R. Luque and S. Marre, *Chem. Soc. Rev.*, 2019, **48**, 3868–3902.
6 J. Theerthagiri, S. J. Lee, K. Karuppasamy, S. Arulmani, S. Veeralakshmi, M. Ashokkumar and M. Y. Choi, *J. Hazard. Mater.*, 2021, **412**, 125245.
7 P. Alulema-Pullupaxi, P. J. Espinoza-Montero, C. Sigcha-Pallo, R. Vargas, L. Fernández, J. M. Peralta-Hernández and J. L. Paz, *Chemosphere*, 2021, **281**, 130821.
8 S. Y. Liou and M. C. Dodd, *Water Res.*, 2021, **200**, 117142.
9 J. J. BelBruno, *Chem. Rev.*, 2019, **119**, 94–119.
10 Z. Han, Y. Xu, H. Tian, J. Liang and D. Sun, *J. Hazard. Mater.*, 2021, **412**, 125145.
11 H. Zhang, *Adv. Mater.*, 2020, **32**, 1806328.
12 Z. Gu, Y. Dong, S. Xu, L. Wang and Z. Liu, *Angew. Chem., Int. Ed.*, 2021, **60**, 2663–2667.
13 K. Haupt, P. X. Medina Rangel and B. T. S. Bui, *Chem. Rev.*, 2020, **120**, 9554–9582.
14 A. Raziq, A. Kidakova, R. Boroznjak, J. Reut, A. Öpik and V. Syritski, *Biosens. Bioelectron.*, 2021, **178**, 113029.
15 N. V. Maksimchuk, I. D. Ivanchikova, K. H. Cho, O. V. Zalomaeva, V. Y. Evtushok, K. P. Larionov, T. S. Glazneva, J. Chang and O. A. Kholdeeva, *Chem. – Eur. J.*, 2021, **27**, 6985–6992.
16 B. Wu, J. Wan, Y. Zhang, B. Pan and I. M. C. Lo, *Environ. Sci. Technol.*, 2020, **54**, 50–66.
17 X. Shen, L. Zhu, J. Li and H. Tang, *Chem. Commun.*, 2007, 1163–1165.
18 X. Shen, L. Zhu, G. Liu, H. Yu and H. Tang, *Environ. Sci. Technol.*, 2008, **42**, 1687–1692.
19 X. Liu, L. Zhu, X. Wang and X. Meng, *Sci. Rep.*, 2020, **10**, 1192.
20 L. Fang, Y. Miao, D. Wei, Y. Zhang and Y. Zhou, *Chemosphere*, 2021, **262**, 128032.
21 A. R. Bagheri, N. Aramash, A. A. Khan, I. Gul, S. Ghotekar and M. Bilal, *J. Environ. Chem. Eng.*, 2020, **9**, 104879.
22 X. Li, B. Yang, K. Xiao, H. Duan, J. Wan and H. Zhao, *Water Res.*, 2021, **203**, 117541.
23 G. Guan, J. H. Pan and Z. Li, *Chemosphere*, 2021, **265**, 129077.
24 L. Pauling, *J. Am. Chem. Soc.*, 1940, **62**, 2643–2657.
25 G. Zerjav, P. Djinovic and A. Pintar, *Catal. Today*, 2018, **315**, 237–246.
26 D. Das and P. Nandi, *Sol. Energy Mater. Sol. Cells*, 2020, **217**, 110674.
27 S. Agrawal, N. J. English, K. R. Thampi and J. M. D. MacElroy, *Phys. Chem. Chem. Phys.*, 2012, **14**, 12044–12056.
28 M. Ismael, *Fuel*, 2021, **303**, 121207.
29 P. Mazierski, A. Mikolajczyk, B. Bajorowicz, A. Malankowska, A. Zaleska-Medynska and J. Nadolna, *Appl. Catal., B*, 2018, **233**, 301–317.
30 X. Pang, N. Skillen, N. Gunaratne, D. W. Rooney and P. K. J. Robertson, *J. Hazard. Mater.*, 2021, **402**, 123461.
31 Y. Ide, Y. Nakasato and M. Ogawa, *J. Am. Chem. Soc.*, 2010, **132**, 3601–3604.
32 Y. Paz, *C. R. Chimie*, 2006, **9**, 774–787.
33 S. Liu, J. Yu and M. Jaroniec, *Chem. Mater.*, 2011, **23**, 4085–4093.
34 X. Shen, L. Zhu, C. Huang, H. Tang, Z. Yu and F. Deng, *J. Mater. Chem.*, 2009, **19**, 4843–4851.
35 C. C. de Escobar, M. A. Lansarin and J. H. Z. dos Santos, *J. Hazard. Mater.*, 2016, **306**, 359–366.
36 J. Guo, X. Fan, Y. Li, S. Yu, Y. Zhang, L. Wang and X. Ren, *J. Hazard. Mater.*, 2021, **415**, 125617.
37 K. Zhao, L. Feng, H. Lin, Y. Fu, B. Lin, W. Cui, H. Li and J. Wei, *Catal. Today*, 2014, **236**, 127–134.
38 E. Tamahkar, M. Bakhshpour and A. Denizli, *J. Biomater. Sci., Polym. Ed.*, 2019, **30**, 450–461.
39 V. R. A. Ferreira, M. A. Azenha, C. M. Pereira and A. F. Silva, *Chem. Eng. J. Adv.*, 2021, **5**, 100071.
40 S. Li, L. Fang, M. Ye and Y. Zhang, *Desalin. Water Treat.*, 2016, **57**, 408–418.
41 X. Liu, L. Zhu, X. Wang, X. Meng and L. Zhong, *J. Nanopart. Res.*, 2020, **22**, 300.
42 M. Cantarella, A. Di Mauro, A. Gulino, L. Spitaleri, G. Nicotra, V. Privitera and G. Impellizzeri, *Appl. Catal., B*, 2018, **238**, 509–517.
43 H. Atarodi and H. Faghihian, *J. Photochem. Photobiol., A*, 2019, **382**, 111892.
44 Z. Lu, G. Zhou, M. Song, X. Liu, H. Tang, H. Dong, P. Huo, F. Yan, P. Du and G. Xing, *Appl. Catal., B*, 2020, **268**, 118433.
45 J. Fang, J. Xu, J. Chen, X. Huang and X. Wang, *Colloids Surf., A*, 2016, **508**, 124–134.
46 A. S. Morshedy, H. R. Ali, A. A. Nada, A. M. Rabie and H. H. El-Maghrabi, *Environ. Technol. Innovation*, 2021, **21**, 101206.
47 Y. Wu, Q. Chen, S. Liu, H. Xiao, M. Zhang and X. Zhang, *Chin. Chem. Lett.*, 2019, **30**, 2186–2190.

48 Y. Wang, Z. Lu, Z. Zhu, X. Zhao, N. Gao, D. Wang, Z. Hua, Y. Yan, P. Huo and M. Song, *RSC Adv.*, 2016, **6**, 51877.

49 F. He, Z. Lu, M. Song, X. Liu, H. Tang, P. Huo, W. Fan, H. Dong, X. Wu and S. Han, *Chem. Eng. J.*, 2019, **360**, 750–761.

50 F. He, Z. Lu, M. Song, M. Liu, H. Tang, P. Huo, W. Fan, H. Dong, X. Wu and G. Xing, *Appl. Surf. Sci.*, 2019, **483**, 453–462.

51 M. Guo, Y. Hu, R. Wang, H. Yu and L. Sun, *Environ. Res.*, 2021, **194**, 110684.

52 C. Zhan, X. Cao, B. Xu, P. Yan, T. Yang, Z. Ye and X. Chen, *Colloid Surf., A*, 2020, **586**, 124244.

53 X. Luo, F. Deng, L. Min, S. Luo, B. Guo, G. Zeng and C. Au, *Environ. Sci. Technol.*, 2013, **47**, 7404–7412.

54 C. C. de Escobar, Y. P. M. Ruiz, M. A. Lasarin, J. H. Z. dos Santos and L. Ye, *Colloid Surf., A*, 2018, **538**, 729–738.

55 W. Li, X. Pei, F. Deng, X. Luo, F. Li and Y. Xiao, *Nanotechnology*, 2015, **26**, 175706.

56 T. S. Anirudhan and S. Madanan Anju, *J. Environ. Chem. Eng.*, 2019, **7**, 103355.

57 C. Lai, M.-M. Wang, C.-M. Zeng, Y.-G. Liu, D.-L. Huang, C. Zhang, R.-Z. Wang, P. Xu, M. Cheng, C. Huang, H.-P. Wu and L. Qin, *Appl. Surf. Sci.*, 2016, **390**, 368–376.

58 Z. Chen, Y. Luo, C. Huang and X. Shen, *Chem. Eng. J.*, 2021, **414**, 128914.

59 J. Yu, C. Zhang, Y. Yang, T. Su, G. Yi and X. Zhang, *Appl. Surf. Sci.*, 2021, **551**, 149476.

60 M. Amiri, K. Dashtian, M. Ghaedi and S. Mosleh, *Photochem. Photobiol. Sci.*, 2020, **19**, 943–955.

61 L. Sun, J. Li, X. Li, C. Liu, H. Wang, P. Huo and Y. Yan, *J. Colloid Interface Sci.*, 2019, **522**, 271–286.

62 J. Bai, R. Shen, Z. Jiang, P. Zhang, Y. Li and X. Li, *Chin. J. Catal.*, 2022, **43**, 359–369.

63 Z. Liang, R. Shen, Y. Hau Ng, P. Zhang, Q. Xiang and X. Li, *J. Mater. Sci. Technol.*, 2020, **56**, 89–121.

64 Z. Wang, X. Liu, W. Li, H. Wang and H. Li, *Ceram. Int.*, 2014, **40**, 8863–8867.

65 S. Chai, G. Zhao, Y.-N. Zhang, Y. Wang, F. Nong, M. Li and D. Li, *Environ. Sci. Technol.*, 2012, **46**, 10182–10190.

66 X. Liu, P. Lv, G. Yao, C. Ma, P. Huo and Y. Yan, *Chem. Eng. J.*, 2013, **217**, 398–406.

67 R. Fiorenza, A. Di Mauro, M. Cantarella, A. Gulino, L. Spitaleri, V. Privitera and G. Impellizzeri, *Mater. Sci. Semicond. Process.*, 2020, **112**, 105019.

68 Y. Wu, Y. Dong, X. Xia, X. Liu and H. Li, *Appl. Surf. Sci.*, 2016, **364**, 829–839.

69 G. Xiao, X. Zhang, W. Zhang, S. Zhang, H. Su and T. Tan, *Appl. Catal., B*, 2015, **170-171**, 255–262.

70 Y. Liu, J. Zhu, X. Liu and H. Li, *RSC Adv.*, 2016, **6**, 69326.

71 L. Zhu, X. Liu, X. Wang and X. Meng, *Sci. Total Environ.*, 2020, **703**, 134732.

72 X. Li, J. Wang, M. Li, Y. Jin, Z. Gu, C. Liu and K. Ogino, *Chin. Chem. Lett.*, 2018, **29**, 527–530.

73 H.-P. Qi and H.-L. Wang, *Appl. Surf. Sci.*, 2020, **511**, 145607.

74 A. Majumder, D. Saidulu, A. K. Gupta and P. S. Ghosal, *J. Environ. Manage.*, 2021, **293**, 112858.

75 Y. Zhang, W. Dai, Y. Wen and G. Zhao, *Appl. Catal., B*, 2017, **212**, 185–192.

76 N. Arbell, K. Bauer and Y. Paz, *ACS Appl. Mater. Interfaces*, 2021, **13**, 39781–39790.

77 X. Shen, L. Zhu, G. Liu, H. Tang, S. Liu and W. Li, *New J. Chem.*, 2009, **33**, 2278–2285.

78 C. Huang, Z. Tu and X. Shen, *J. Hazard. Mater.*, 2013, **248–249**, 379–386.

79 D. Sharabi and Y. Paz, *Appl. Catal., B*, 2010, **95**, 169–178.

80 X. Shen, L. Zhu, N. Wang, T. Zhang and H. Tang, *Catal. Today*, 2014, **225**, 164–170.

81 Q. Yuan, D. Zhang, P. Yu, R. Sun, H. Javed, G. Wu and P. J. J. Alvarez, *Environ. Sci. Technol.*, 2020, **54**, 4621–4630.

82 G. Zhou, Y. Cao, Y. Jin, C. Wang, Y. Wang, C. Hua and S. Wu, *J. Cleaner Prod.*, 2020, **274**, 122929.

83 L. Li, X. Zheng, Y. Chi, Y. Wang, X. Sun, Q. Yue, B. Gao and S. Xu, *J. Hazard. Mater.*, 2020, **383**, 121211.

84 L. Bao, M. Meng, K. Sun, W. Li, D. Zhao, H. Li and M. He, *J. Appl. Polym. Sci.*, 2014, **131**, 40890.

85 Y. Huang, P. Wang, F. Chen, G. Zhou, M. Song, X. Liu, C. Ma, S. Han, Y. Yan and Z. Lu, *J. Photochem. Photobiol., A*, 2021, **410**, 113159.

86 H. K. Melvin, Ng, C. P. Leo and A. Z. Abdullah, *J. Environ. Chem. Eng.*, 2017, **5**, 3991–3998.

87 S. M. Amorim, G. Steffen, J. M. D. S. Junior, C. Z. Brusamarello, A. P. Romio and M. D. Domenico, *Polym. Polym. Compos.*, 2020, **29**, 1055–1074.

88 F. Deng, Y. Li, X. Luo, L. Yang and X. Tu, *Colloids Surf., A*, 2012, **395**, 183–189.

89 Y. Luo, Z. Lu, Y. Jiang, D. Wang, L. Yang, P. Huo, Z. Da, X. Bai, X. Xie and P. Yang, *Chem. Eng. J.*, 2014, **240**, 244–252.

90 A. Shahnazi, M. R. Nabid and R. Sedghi, *React. Funct. Polym.*, 2020, **151**, 104580.

91 Z. Lu, Z. Yu, J. Dong, M. Song, Y. X. Liu, Z. Ma, H. Su, Y. Yan and P. Huo, *Chem. Eng. J.*, 2018, **337**, 228–241.

92 H. Tang, L. Zhu, C. Yu and X. Shen, *Sep. Purif. Technol.*, 2012, **95**, 165–171.

93 Z. Lu, F. Chen, M. He, M. Song, Z. Ma, W. Shi, Y. Yan, J. Lan, F. Li and P. Xiao, *Chem. Eng. J.*, 2014, **249**, 15–26.

94 C. Zhang, H. Chen, M. Ma and Z. Yang, *J. Mol. Catal. A: Chem.*, 2015, **402**, 10–16.

95 L. Xu, J. Pan, Q. Xia, F. Shi, J. Dai, X. Wei and Y. Yan, *J. Phys. Chem. C*, 2012, **116**, 25309–25318.

96 W. Xing, L. Ni, X. Liu, Y. Luo, Z. Lu, Y. Yan and P. Huo, *RSC Adv.*, 2013, **3**, 26334–26342.

97 G. Chen, S. He, G. Shi, Y. Ma, C. Ruan., X. Jin, Q. Chen, X. Liu, H. Dai, X. Chen and D. Huang, *Chem. Eng. J.*, 2021, **423**, 130184.

98 L. Wan, H. Liu, C. Huang and X. Shen, *J. Mater. Chem. A*, 2021, **8**, 25931–25940.

99 C. Zhang, S. Si and Z. Yang, *Sep. Purif. Technol.*, 2015, **143**, 88–93.

100 Z. Lu, J. Peng, M. Song, Y. Liu, X. Liu, P. Huo, H. Dong, S. Yuan, Z. Ma and S. Han, *Chem. Eng. J.*, 2019, **360**, 1262–1276.

101 J. Peng and G. Huang, *Chem. Commun.*, 2019, **106**, 202–210.

102 X. Gao, J. Liu, M. Li, C. Guo, H. Long, Y. Zhang and L. Xin, *Chem. Eng. J.*, 2020, **385**, 123897.

103 Y. Zhang, J. Shang, Y. Song, C. Rong, Y. Wang, W. Huang and K. Yu, *Water Sci. Technol.*, 2017, **75**, 659–669.

104 X. Li, J. Wan, Y. Wang, H. Chi, Z. Yan and S. Ding, *Chemosphere*, 2020, **240**, 124875.

105 M. Huang, T. Zhou, X. Wu and J. Mao, *Chin. J. Chem. Eng.*, 2015, **23**, 1698–1704.

106 M. Chen, J. Lu, J. Gao, C. Yu, W. Xing, J. Dai, M. Meng, Y. Yan and Y. Wu, *J. Membr. Sci.*, 2022, **642**, 119994.

107 H. Zhao, Q. Wang, Y. Chen, Q. Tian and G. Zhao, *Carbon*, 2017, **124**, 111–122.

108 Y. Song, C. Rong, J. Shang, Y. Wang, Y. Zhang and K. Yu, *J. Chem. Technol. Biotechnol.*, 2017, **92**, 2038–2049.

109 P. Haller, I. Machado, J. Torres, A. Vila and N. Veiga, *Polymers*, 2021, **13**, 3127.

110 Z. Chen, X. Liu, C. Huang, J. Li and X. Shen, *ACS Appl. Mater. Interfaces*, 2020, **12**, 6615–6626.

111 Y. Xie, J. Wan, Z. Yan, Y. Wang, T. Xiao, J. Hou and H. Chen, *Chem. Eng. J.*, 2022, **429**, 132237.

112 C. Zeng, Y. Wang, T. Xiao, Z. Yan, J. Wan and Q. Xie, *J. Hazard. Mater.*, 2022, **424**, 127499.

113 X. Li, J. Wan, Y. Wang, Z. Yan, H. Chi and S. Ding, *Appl. Catal., B*, 2020, **266**, 118591.

114 X. Li, J. Wan, Y. Wang, S. Ding and J. Sun, *Chem. Eng. J.*, 2021, **413**, 127406.

115 S. Ding, J. Wan, Y. Wang, Z. Yan and Y. Ma, *Chem. Eng. J.*, 2021, **422**, 130406.

116 S. Ding, J. Wan, Y. Ma, Y. Wang, X. Li, J. Sun and M. Pu, *Chemosphere*, 2021, **270**, 128620.

117 H. Chi, C. Li, M. Huang, J. Wan, X. Zhou and B. Yan, *Chem. Eng. J.*, 2021, **424**, 130367.

118 K. K. Abbas and A. M. H. A. Al-Ghaban, *J. Environ. Chem. Eng.*, 2019, **7**, 103168.

119 X. Yin, J. Long, Y. Xi and X. Luo, *ACS Sustainable Chem. Eng.*, 2017, **5**, 2090–2097.

120 Z. Guo, W. Wei, Y. Li, Z. Li, F. Hou and A. Wei, *J. Hazard. Mater.*, 2022, **422**, 126946.

121 X. Zhao, M. Li and Y. Liu, *Microorganisms*, 2019, **7**, 381.

122 V. Svitkova and I. Palchetti, *Bioelectrochemistry*, 2020, **136**, 107590.

123 M. A. Beluomini, J. L. da Silva, A. C. deSa, E. Buffon and T. C. Pereira, *J. Electroanal. Chem.*, 2019, **840**, 343–366.

124 C. Zhang, S. Si and Z. Yang, *Biosens. Bioelectron.*, 2015, **65**, 115–120.

125 C. Zhang, S. Si and Z. Yang, *Sens. Actuators, B*, 2015, **211**, 206–212.

126 C. Zhang, W. Bai and Z. Yang, *Electrochim. Acta*, 2016, **187**, 451–456.

127 C. Gao, Y. Wang, S. Yuan, J. Xue, B. Cao and J. Yu, *Biosens. Bioelectron.*, 2017, **90**, 336–342.

128 M. Liu, X. Ding, Q. Yang, Y. Wang, G. Zhao and N. Yang, *J. Hazard. Mater.*, 2017, **331**, 309–320.

129 J. Cen, P. Gao, H. Wang, L. Han, Y. Zhang, P. Wang and N. Jia, *J. Mater. Chem. C*, 2018, **6**, 3937–3944.

130 H. Shi, Y. Wang, J. Zhao, X. Huang and G. Zhao, *J. Hazard. Mater.*, 2018, **342**, 131–138.

131 J. Wang, Q. Xu, W. W. Xia, Y. Shu, D. Jin, Y. Zang and X. Hu, *Sens. Actuators, B*, 2018, **217**, 215–224.

132 Q. Kong, Y. Wang, L. Zhang, C. Xu and J. Yu, *Biosens. Bioelectron.*, 2018, **110**, 58–64.

133 X. Wang, H. Deng, C. Wang, Q. Wei, Y. Wang, X. Xiong, C. Li and W. Li, *Analyst*, 2020, **145**, 1302–1309.

134 K. Dashtian, S. Hajati and M. Ghaedi, *Biosens. Bioelectron.*, 2020, **165**, 112346.

135 M. L. Yola, C. Gode and N. Atar, *Electrochim. Acta*, 2017, **246**, 135–140.

136 G. Cai, Z. Yu and D. Tang, *Talanta*, 2020, **219**, 121341.

137 X. Ren, L. Yang, Y. Li and X. Li, *Appl. Surf. Sci.*, 2021, **544**, 148879.